Chinese Journal of Catalysis 36 (2015) 2219–2228

available at www.sciencedirect.com

ScienceDirect

journal homepage: www.elsevier.com/locate/chnjc

Article (Special Issue on Photocatalysis)

Facile synthesis of Ag_2O-TiO_2/sepiolite composites with enhanced visible-light photocatalytic properties

Yu Du [a], Dandan Tang [a], Gaoke Zhang [a,b,*], Xiaoyong Wu [a]

[a] *School of Resources and Environmental Engineering, Wuhan University of Technology, 122 Luoshi Road, Wuhan 430070, Hubei, China*

[b] *State Key Laboratory of Silicate Materials for Architectures, Wuhan University of Technology, 122 Luoshi Road, Wuhan 430070, Hubei, China*

ARTICLE INFO

Article history:
Received 17 August 2015
Accepted 11 November 2015
Published 20 December 2015

Keywords:
Silver oxide
Titanium dioxide
Sepiolite
Heterostructure
Photocatalysis
Acid red G
Photocatalytic mechanism

ABSTRACT

Ag_2O-TiO_2/sepiolite heterostructure composites were synthesized by a simple two-step method at low temperatures (100–450 °C). Acid red G aqueous solution and gaseous formaldehyde were chosen as model organic pollutants to evaluate the photocatalytic performance of the as-prepared composites. The results showed that the Ag_2O-TiO_2/sepiolite exhibited enhanced photocatalytic activity over pure Ag_2O-TiO_2, TiO_2/sepiolite, and Ag_2O/sepiolite under visible-light irradiation (λ > 420 nm). The excellent photocatalytic efficiency of these composites can be ascribed to the synergistic effect between the heterojunction and the porous structure of the clay layers, which induced high adsorption and efficient charge separation. In addition, the active species involved in the degradation reaction have been investigated by photoluminescence spectroscopy and quenching experiments. A possible photocatalytic degradation mechanism of acid red G dye by the Ag_2O-TiO_2/sepiolite composite is also discussed.

1. Introduction

Photocatalysis technology is considered a promising method for air and sewage purification because it is efficient, economical, and environmentally viable [1–6]. Titanium dioxide (TiO_2) has also received increased attention because of its nontoxicity, high chemical stability, and low cost [7–9]. However, TiO_2 can only exhibit photocatalytic activity under UV light. Furthermore, its poor adsorption capacity and high recombination rate of photogenerated electron-hole pairs hinder its practical application [10–12]. To resolve this problem, various methods, such as chemical modification [13], metallization [14], and the development of novel heterostructure semiconductors [15,16], have been employed to enhance the charge-separation efficiency. For example, Tang et al. [17] reported that the Ag/AlO_2/TiO_2 heterojunction presented higher photocatalytic activity for decomposing formaldehyde under sunlight irradiation than did pure TiO_2 and $AgAlO_2$. This was attributed to the heterojunction providing a matching energy band structure. Lee et al. [18] found that TiO_2/CuO nanofiber exhibited high photocatalytic properties for degrading and cleaning the organics produced from dye wastewater, which can be ascribed to the high quantum efficiency.

In addition, researchers have found that silver oxide (Ag_2O) can act as a novel visible-light-driven semiconductor material because of its unique band gap, good sensitivity to light, facile preparation, and inexpensiveness, meaning that this could be an excellent charge-separation promoter and built-in acceptor [19–21]. Ag particles are also used as a cleaning agent to remove bacteria from contaminated water [22–24]. Theoretically, the conduction band (CB) of Ag_2O is more negative than the corresponding band of TiO_2, and the valence band (VB) of TiO_2

* Corresponding author. Tel: +86-27-87651816; Fax: +86-27-87887445; E-mail: gkzhang@whut.edu.cn
This work was supported by the National Key Technology R&D Program of China (2012BAJ25B02-03).
DOI: 10.1016/S1872-2067(15)61015-4 | http://www.sciencedirect.com/science/journal/18722067 | Chin. J. Catal., Vol. 36, No. 12, December 2015

is more positive than that of Ag_2O [25]. Their matching band gaps and positions might favor the formation of Ag_2O-TiO_2 heterostructures, which expands the photoabsorption range and facilitates the separation of photogenerated electrons and hole pairs [26–31]. However, their application is also limited by weak adsorption and the difficulty in separating them from wastewater.

Sepiolite is a microfibrous clay mineral consisting of a 2:1 layered structure built by two tetrahedral silica sheets with a central magnesia sheet [32]. Its peculiar structural tunnels lead to interesting surface properties and high absorption capacity [33]. Zhang et al. [34] studied bicrystalline TiO_2 by supporting it on porous sepiolite clay for the photocatalytic degradation of gaseous formaldehyde, wherein the TiO_2/sepiolite showed a higher photocatalytic activity than commercial Degussa P-25 or bare TiO_2. Moreover, the layered structure of sepiolite exhibited higher physicochemical stability. Thus, sepiolite may also be a good support for the Ag_2O-TiO_2 heterojunction catalyst, which can improve the catalyst adsorption capacity and catalyst separation, and its recycling from wastewater.

In the present work, heterostructure Ag_2O-TiO_2/sepiolite composites were synthesized by a simple two-step method. Their photocatalytic activities were investigated by the photocatalytic degradation of acid red G (ARG) aqueous solution and gaseous formaldehyde under visible-light irradiation (λ > 420 nm). The structural features of the composites were analyzed through systematic characterization, and the visible-light photocatalytic mechanism of the Ag_2O-TiO_2/sepiolite composites is discussed in detail.

2. Experimental

2.1. Catalyst prepartation

The sepiolite sample used in this study was from Hunan Province, China. All chemical reagents were of analytical grade and used without further purification. The synthesis of Ag_2O-TiO_2/sepiolite composite comprises two main processes.

TiO_2 sol was prepared by an acid-catalyzed sol-gel method from a $TiCl_4$ precursor (Sinopharm Chemical Reagent Co., Ltd., China). $TiCl_4$ (8 mL) was added gradually to a HCl solution (22 wt%) under continuous stirring for 0.5 h at 25 °C, and then aged for 6 h to obtain a transparent TiO_2 sol. Then, the TiO_2 sol was added dropwise into sepiolite powder saturated with deionized water (1 wt%) under vigorous stirring for 0.5 h at 70 °C, before being aged for 12 h to obtain individual TiO_2 loadings of 30 wt% on the sepiolite support (30%TiO_2/sepiolite). The resulting mixed suspensions were centrifuged at 5000 r/min several times and then washed with deionized water to neutralize the supernatants until no Cl^- was detected by $AgNO_3$ solution. After removing all excessive chloride, the samples were dried at 70 °C for 5 h.

Ag_2O-TiO_2/sepiolite composites were synthesized via an impregnation method. TiO_2/sepiolite powder (1.00 g) was dispersed in 18.5 mL of $AgNO_3$ solution (0.05 mol/L) to produce a suspension (Ag/powders = 10 wt%). After stirring in the dark for 2 h, the resulting suspension was dried at 60 °C and then calcined at 100, 200, 350, and 450 °C for 30 min under ambient conditions. The resulting samples were stored in the dark in the form of fine white powders (< 400 °C), in which the Ag_2O phase may exist on the surface of the TiO_2/sepiolite composites. The color of the Ag_2O-TiO_2/sepiolite composites changed to gray by increasing the calcination temperature to 450 °C, owing to the decomposition of Ag_2O to metallic Ag [25]. For comparison and to investigate the effect of Ag_2O particles on the photocatalytic performance of sepiolite clay, pure Ag_2O-TiO_2 and Ag_2O/sepiolite composites were also prepared following the same procedure to provide 10%Ag_2O-30%TiO_2/sepiolite (200 °C).

2.2. Catalyst characterization

X-ray diffraction (XRD, Rigaku D/MAX-RB diffractometer, operating at 40 kV and 50 mA with Cu K_α radiation, λ = 0.15406 nm) was used to determine the structure and crystallinity of the as-prepared samples. X-ray photoelectron spectroscopy (XPS) data were collected using an ESCALAB II XPS system operating in hybrid mode, with a monochromatic Mg K_α source and a charge neutralizer. All binding energies obtained by the XPS spectral analysis used the C 1*s* peak at 284.5 eV as a reference. The morphologies of the samples were observed by scanning electronic microscopy (SEM, JSM5610LV). The absorption edge of the samples was measured by an ultraviolet-visible (UV-vis) spectrophotometer (UV-2550, Shimadzu), for which the raw sepiolite and TiO_2-supported catalyst samples were used as the reflectance standard. A N_2 adsorption-desorption isotherm was obtained at liquid nitrogen temperature (–196 °C) using a Quantachrome AUTOSORB-1 nitrogen adsorption apparatus. The specific surface area was determined by the multi-point BET method and the pore sizes were measured by the BJH method of adsorption. The Fourier transform infrared (FT-IR) spectra of the chemical bonds on the surface of the samples were obtained using a Thermo Nicolet Nexus spectrometer. Photoluminescence (PL) spectra were recorded via a fluorescence spectrophotometer (RF-5301PC, Shimadzu) with an excitation wavelength of 312 nm, which is capable of detecting the hydroxyl radical (•OH) during the photocatalytic degradation process.

2.3. Photocatalytic activity measurements

The photocatalytic degradation experiments of ARG dye and gaseous formaldehyde were performed under visible-light irradiation at room temperature. A desired amount (0.15 g) of the as-prepared catalyst was homogeneously suspended in the ARG dye aqueous solution (100 mg/L) under continuous stirring for 30 min in a dark environment to establish the adsorption-desorption equilibrium. The reaction was started by direct exposure to visible-light irradiation (300 W Dy lamp) with a 420-nm cutoff filter. At given time intervals of illumination, small aliquots of the stirred suspension were drawn and centrifuged to remove the photocatalyst. The supernatant liquor of the ARG dye was analyzed by UV-vis spectrophotometry (UV751GD, China) at its maximum absorption wavelength

(λ_{max}) of 505 nm.

Gaseous formaldehyde degradation was conducted in a closed stainless steel photoreactor with an inner volume of 0.8 L. The as-prepared catalyst, with a dosage of 0.15 g, was dispersed in a dish of diameter 70 mm. Then the sample was set into the gas photoreactor, and formaldehyde solution (2 μL) was injected into the photoreactor by microsyringe. The reactor was blown by a fan for the formaldehyde to slowly volatilize until the initial concentration reached equilibrium. After several minutes, a 300 W Dy lamp was turned on to irradiate the photoreactor with a 420-nm cutoff filter. A 1412 photoacoustic field gas-monitor (Innova AirTech Instruments, Denmark) was applied to detect the concentration of gaseous formaldehyde, and the mineralization products (CO_2 and H_2O) were also monitored. The tests were performed at room temperature (25 °C).

3. Results and discussion

3.1. Photocatalyst characterization

XRD was used to investigate the crystal structure of the catalyst particles. Fig. 1(a) shows the XRD patterns over a scan range of 5° to 70° for the sepiolite, TiO_2/sepiolite, and Ag_2O-TiO_2/sepiolite composites obtained at different temperatures. It is found that all samples show the main phase of sepiolite, for which the diffraction peaks at 2θ = 8.78°, 12.2°, 24.8°, and 26.6° are indexed to the (110), (130), (231), and (080) planes, respectively, of the pristine sepiolite (JCPDS 26-1226).

Meanwhile, the intensities of the (130), (231), and (080) peaks of the sepiolite gradually decreased by increasing the calcination temperature, which indicates that the layered structure of sepiolite was, to some extent, destroyed [35,36]. In addition, the diffraction peaks at 2θ = 25.3°, 48.1°, and 55.1° are indexed to the (101), (200), and (211) planes, respectively, of the anatase phase of TiO_2 (JCPDS 83-2243), whereas the peaks at 2θ = 27.4° and 36.0° are indexed to the (110) and (101) planes, respectively, of the rutile phase of TiO_2 (JCPDS 78-2485) [37]. There are commonly two naturally occurring phases of titania (rutile and anatase) when the calcination temperature is above 400 °C [33], and the thermal stability of the anatase crystalline phase for Ag_2O-TiO_2/sepiolite composites can likely be attributed to the stabilizing effect of the silica that exists in the sepiolite framework [32]. In Fig. 1(a), the peaks corresponding to the Ag_2O phase are not clearly detectable. To further demonstrate the phase structures of the Ag on the surface of the sepiolite, the weak diffraction peaks of Ag_2O at 2θ = 32.7° (JCPDS 12-0793) and metallic Ag at 2θ = 44.3° (JCPDS 04-0783) were further detected, as shown in Fig. 1(b) and (c). The samples obtained at 200 and 350 °C were found to contain the Ag_2O phase (Fig. 1(b)). Metallic Ag was observed as the calcination temperature was increased to 450 °C (Fig. 1(c)), which can be attributed to the decomposition of Ag_2O [38]. In this study, TiO_2 could exist as a mixture of nanosized anatase and rutile in the composites, and the formation of the Ag_2O phase could be inhibited by controlling the calcination temperature below 450 °C.

XPS was employed to analyze the chemical state of the elements on the surface of the Ag_2O-TiO_2/sepiolite composites, and the results are shown in Fig. 2(a). In Fig. 2(b), the Ag 3*d* region shows XPS peaks with two individual peaks at 368.3 and 374.3 eV, which are assigned to the Ag $3d_{5/2}$ and Ag $3d_{3/2}$ peaks in Ag_2O phase [39,40], respectively. In Fig. 2(c), the Ti 2*p* region exhibits two individual peaks at 458.7 and 464.3 eV, which indicate that Ti^{4+} of TiO_2 is the major Ti species in the Ag_2O-TiO_2/sepiolite composites [41–43]. In addition, it can be seen that the binding energy values of the Ti 2*p* region are slightly increased, which is attributed to the interaction of Ag ions with the TiO_2 surface [44,45]. In Fig. 2(d), the main peak of the O 1*s* region with a binding energy of 530.1 eV is assigned to the oxygen in the TiO_2 crystal lattice [38,39,43], while the peak at 532.4 eV is assigned to the metal–OH bonds [46]. The formation of silver oxide is attributed to the Ag^+ ions absorbing oxygen ions originating from the TiO_2 metal crystal lattice or from dispersed –OH in the clay [47].

The morphologies of the sepiolite, TiO_2/sepiolite, and Ag_2O-TiO_2/sepiolite composites were characterized by SEM. In Fig. 3(a), the sepiolite exhibits a smooth and flat surface, while the TiO_2/sepiolite composite presents a relatively rough and loose-knit section (Fig. 3(b)). From Fig. 3(c), it can be seen that a large number of the TiO_2 and Ag_2O particles assembled on the

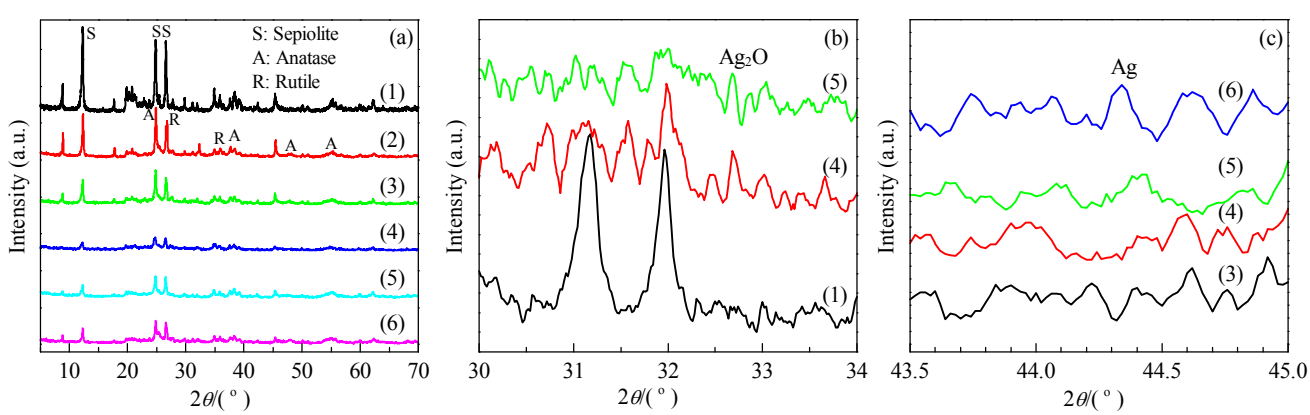

Fig. 1. (a) XRD patterns of sepiolite (1), TiO_2/sepiolite (2), Ag_2O-TiO_2/sepiolite (100 °C) (3), Ag_2O-TiO_2/sepiolite (200 °C) (4), Ag_2O-TiO_2/sepiolite (350 °C) (5), and Ag_2O-TiO_2/sepiolite (450 °C) (6); The corresponding enlarged diffraction areas from 30° to 34° (b) and 43.5° to 45° (c) for some typical samples.

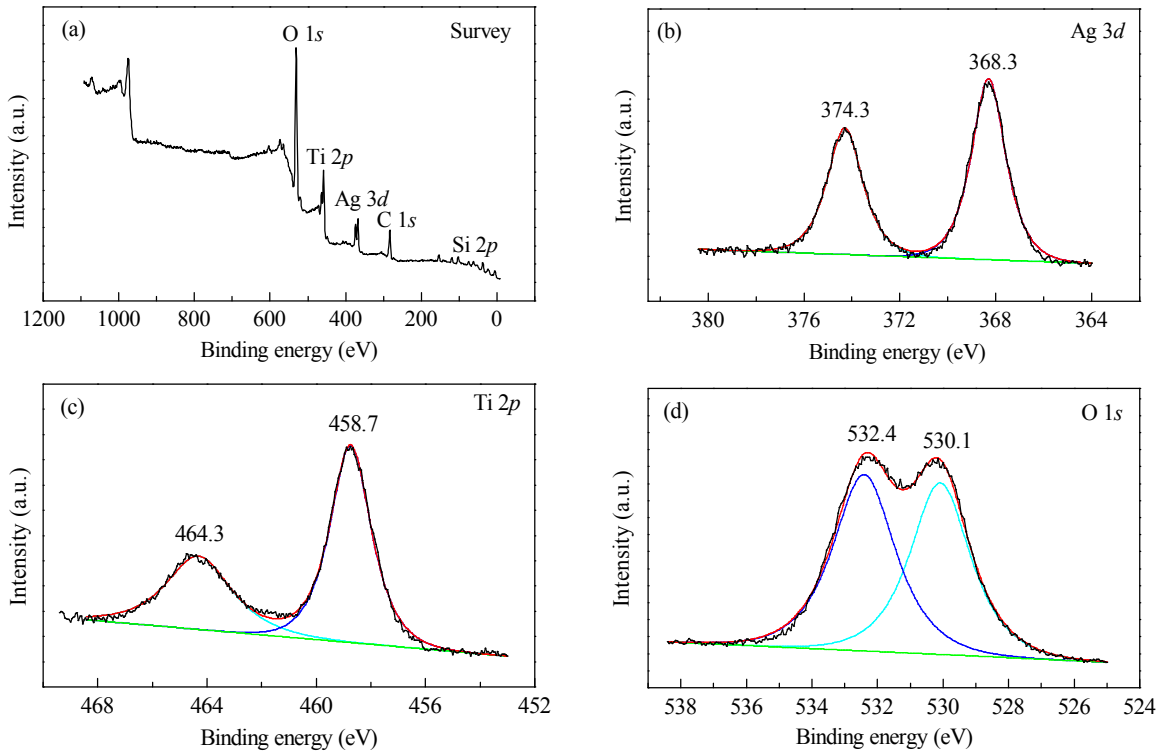

Fig. 2. XPS spectrum of Ag_2O-TiO_2/sepiolite composites (a) and high-resolution XPS spectra of Ag 3*d* region (b), Ti 2*p* region (c), and O 1*s* region (d).

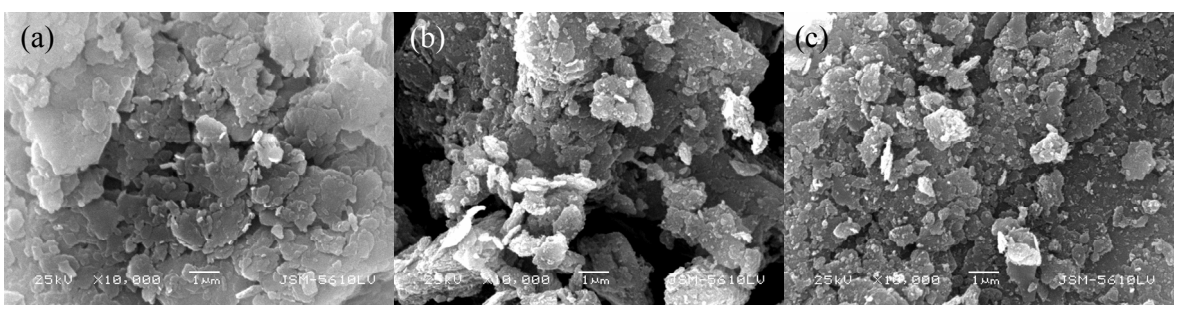

Fig. 3. SEM images of raw sepiolite (a), TiO_2/sepiolite (b), and Ag_2O-TiO_2/sepiolite composites (c).

surface of the sepiolite, and their shapes are quite irregular. The morphology of the sepiolite clay shows no obvious difference, while the layered structures of the mineral congeries were partially destroyed when the TiO_2 nanoparticles were introduced into the sepiolite by the sol-gel process.

HRTEM was used to further investigate the phase structure of the Ag_2O-TiO_2/sepiolite composite. Fig. 4(a) and (b) show typical TEM images of the Ag_2O-TiO_2/sepiolite composite with a layered structure, which is consistent with the SEM observations. Fig. 4(c) and (d) show HRTEM images recorded from the white framed areas indicated in Fig. 4(b), in which it can be seen that two crystals of Ag_2O and TiO_2 are tightly interconnected, and the lattice fringe spacing of 0.272 nm (Fig. 4(c)) corresponds to the (111) crystallographic plane of Ag_2O. The observed lattice spacings of 0.351 and 0.324 nm (Fig. 4(d)) correspond to the (101) plane of the anatase and the (110) plane of the rutile phase, respectively. The HRTEM images further confirm that heterostructures of Ag_2O and TiO_2 have been formed in the composites [48].

The N_2 adsorption-desorption isotherm and pore size distribution curve of the Ag_2O-TiO_2/sepiolite composite (200 °C) are shown in Fig. 5. The BET surface area, pore volume, and average pore size of the different samples are summarized in Table 1. The surface area (60.39 m^2/g) of the Ag_2O-TiO_2/sepiolite composite prepared at 200 °C is five times higher than that of the raw sepiolite (12.21 m^2/g). Taking into account the calcination temperature, Ag_2O-TiO_2/sepiolite composites show a higher thermal stability and a loss of specific surface area of between 15% and 33% [49]. The N_2 adsorption-desorption isotherm of the composite seems to be type IV, according to the IUPAC classification, which demonstrates the presence of mesopores (2–50 nm) [26]. The shape of the hysteresis loops is of type H3, which is the main feature of a multiporous structure [32,50]. The continuously increased adsorption branch at relative pressure (p/p_0 = 0.01–1.0) indicates capillary condensation of N_2 molecules inside the different pore-sized structure (micropores and mesoporous) [50–52].

Typical FT-IR spectra of sepiolite and the Ag_2O-TiO_2/sepio-

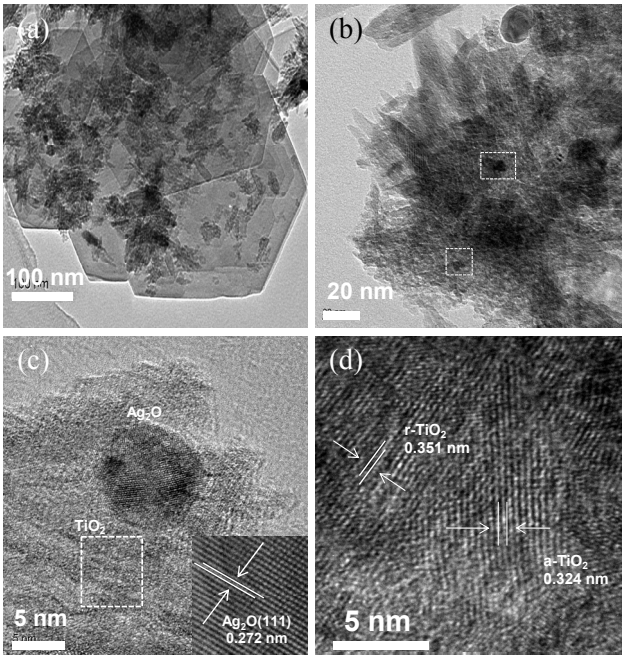

Fig. 4. TEM (a,b) and HRTEM (c,d) images of the Ag_2O-TiO_2/sepiolite composite prepared at 200 °C.

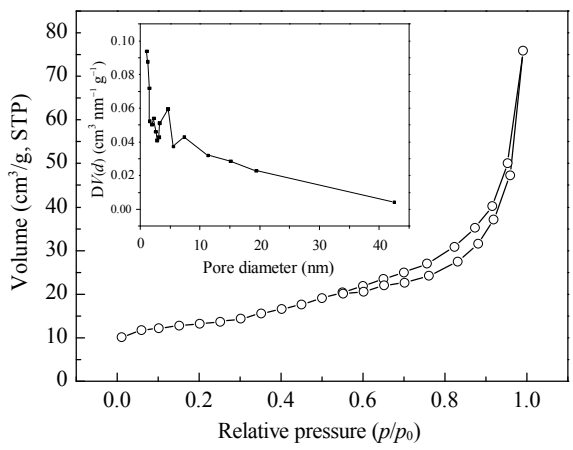

Fig. 5. N_2 adsorption-desorption isotherm of the Ag_2O-TiO_2/sepiolite composite prepared at 200 °C. The inset is the corresponding pore size distribution.

lite composite before and after photocatalytic degradation of ARG dye are illustrated in Fig. 6. The bands observed at 3668 cm^{-1} can be attributed to the stretching vibrations of hydroxyl groups (Mg_3OH) and water molecules bound to the octahedral sheets of Mg ions in the sepiolite clay [53–55]. The bands between 3435 and 1637 cm^{-1} can be assigned to the O–H stretching mode and the H–O–H bending mode from the interbedded water molecule of the clay [37]. The bands at 1114 and 1033 cm^{-1} are due to the stretching of Si–O in the Si–O–Si groups of the tetrahedral sheet, and the peak at 637 cm^{-1} is assigned to OH bending vibrations [56]. As reported, the Si–O–Al (octahedral) bending vibrations are present at 469 cm^{-1} [57]. As shown in Fig. 6(b), the disappearance of the band at 430 cm^{-1} is assigned to Si–O–Si bending vibrations [54], and the shift of the bands at 3424 and 1631 cm^{-1} might be caused

Table 1
Specific surface areas and pore parameters of sepiolite, TiO_2/sepiolite, Ag_2O-TiO_2, and the Ag_2O-TiO_2/sepiolite composites prepared at different temperatures.

Sample	BET surface area (m^2/g)	Pore volume (cm^3/g)	Average pore size (nm)
Sepiolite	12.21	0.06	69.46
TiO_2/sepiolite	63.21	0.10	37.60
Ag_2O-TiO_2	3.13	0.01	42.19
Ag_2O-TiO_2/sepiolite (100 °C)	51.21	0.09	71.29
Ag_2O-TiO_2/sepiolite (200 °C)	60.39	0.10	43.66
Ag_2O-TiO_2/sepiolite (350 °C)	40.44	0.07	47.74
Ag_2O-TiO_2/sepiolite (450 °C)	44.99	0.07	90.60

by changes to the chemical bond vibration for TiO_2 particles inserted into the layer of sepiolite or the bonding of Ti–OH [58], indicating that the layered structure of sepiolite has been destroyed during the preparation process. Moreover, the characteristic bands of Si–O in the Si–O–Si groups of the tetrahedral sheets (around 1114, 1033, and 469 cm^{-1}) still exist, and the new peak at 908 cm^{-1} is caused by a Ti–O–H stretching vibration. In addition, the intensities of the vibration modes at 637–1033 cm^{-1} are decreased, which indicates that the organic matter on the clay was removed in the calcination process. The FT-IR spectrum of the recovered composite does not show the characteristic peak of ARG dye, which confirms that other than that which was adsorbed by the composite, the ARG was degraded completely by the photocatalysis. Meanwhile, the result also indicates that the Ag_2O-TiO_2/sepiolite composite has good stability.

The UV-vis diffuse reflectance spectra of sepiolite, TiO_2, Ag_2O, TiO_2/sepiolite, and Ag_2O-TiO_2/sepiolite composite are shown in Fig. 7. The absorption edge of the Ag_2O-TiO_2/sepiolite composite tends to red-shift compared with that of the TiO_2/sepiolite sample. The band gaps of pure TiO_2 and pure Ag_2O are calculated to be 2.9 and 1.0 eV, respectively. The Ag_2O-TiO_2/sepiolite composite exhibited enhanced photoabsorption from the UV light region to the visible-light region in the range 370–430 nm. The results indicate that the Ag_2O na-

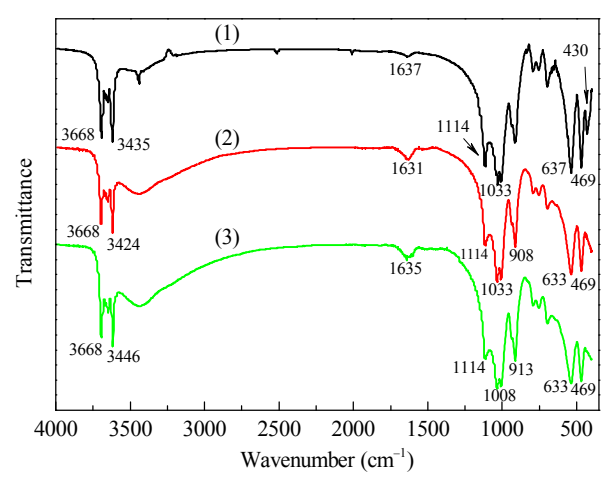

Fig. 6. FT-IR spectra of sepiolite (1) and the Ag_2O-TiO_2/sepiolite composite before (2) and after (3) photocatalytic reaction.

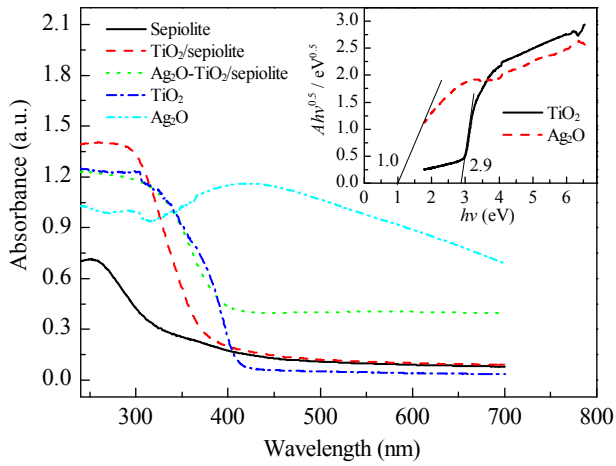

Fig. 7. UV-vis diffuse reflectance spectra of sepiolite, TiO_2, Ag_2O, TiO_2/sepiolite, and Ag_2O-TiO_2/sepiolite composite.

noparticles loaded onto the TiO_2/sepiolite have a suitable band gap for photocatalytic decomposition of organic pollutants in the visible-light region.

3.2. *Photocatalytic activity of Ag_2O-TiO_2/sepiolite composite*

The photocatalytic activities of the Ag_2O-TiO_2/sepiolite composites were evaluated by photocatalytic degradation of ARG dye solution and gaseous formaldehyde under visible-light irradiation. As shown in Fig. 8, it is clear that the TiO_2/sepiolite composites showed little photocatalytic performance. However, after coating Ag_2O nanoparticles, the Ag_2O-TiO_2/sepiolite composites showed an obviously enhanced photocatalytic activity and ARG was completely decomposed with an increase in irradiation time. Specifically, when the calcination temperature is 200 °C, the obtained Ag_2O-TiO_2/sepiolite composite shows superior photocatalytic activity and the concentration of ARG was decreased by 98% after 40 min, whereas only about 24% of ARG could be removed over the TiO_2/sepiolite after 40 min irradiation. Furthermore, the photocatalytic degradation of the ARG solution followed a pseudo-first-order reaction rate [59]. Thus, the rate constant (k, min^{-1}) of the ARG decomposition over Ag_2O-TiO_2/sepiolite composites can be estimated by

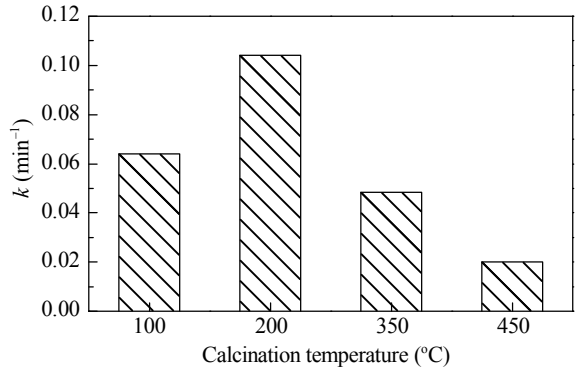

Fig. 9. Comparison of apparent rate constants for the Ag_2O-TiO_2/sepiolite catalysts calcined at different temperatures for the degradation of ARG solution.

$\ln(C_0/C) = kt$. Fig. 9 shows the comparison of the apparent rate constants of the Ag_2O-TiO_2/sepiolite composites at different calcined temperatures for the degradation of ARG solution. The k values for the ARG decomposition by the catalysts calcined at 100, 200, 350, and 450 °C are 0.064, 0.104, 0.048, and 0.020 min^{-1}, respectively. Fig. 10 shows the photocatalytic activities of the samples with different amounts of Ag_2O under visible-light irradiation. It is clearly shown that the samples with a content of Ag_2O from 2% to 10% exhibited enhanced photocatalytic activity. However, when the content of Ag_2O was further increased to 15%, no further enhancement of ARG degradation can be observed. Hence, when the content of Ag_2O was increased to 10%, a heterostructure of Ag_2O and TiO_2 was formed on the surface of sepiolite, which made the photocatalytic process more efficient.

Fig. 11 displays the photocatalytic degradation of the ARG solution by the different photocatalysts. It is clear that the Ag_2O-TiO_2/sepiolite composite exhibited the highest photocatalytic activity of the systems studied. ARG is almost completely degraded after 40 min irradiation over Ag_2O-TiO_2/sepiolite under visible light, whereas only about 7% of ARG could be removed over P-25, 11% over pure sepiolite, 24% over TiO_2/sepiolite, 62% over TiO_2-Ag_2O, and 87% over Ag_2O/sepiolite after 40 min irradiation. Therefore, it is possible that a steady system is formed between Ag_2O and TiO_2 nanoparticles

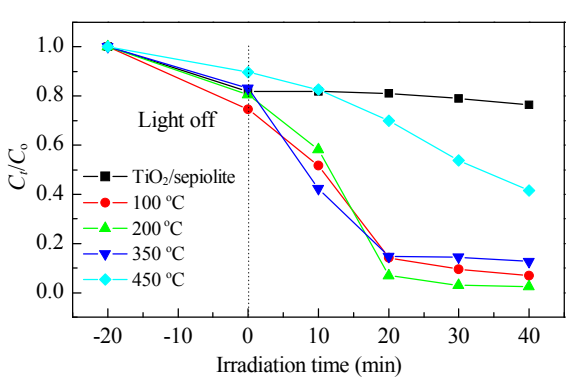

Fig. 8. Photocatalytic degradation of ARG by TiO_2/sepiolite and the Ag_2O-TiO_2/sepiolite catalysts obtained at different temperatures under visible-light irradiation.

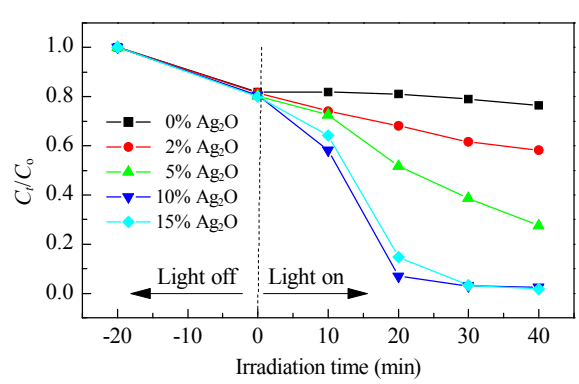

Fig. 10. Visible-light photocatalytic degradation of ARG by Ag_2O-TiO_2/sepiolite catalysts with different Ag_2O contents.

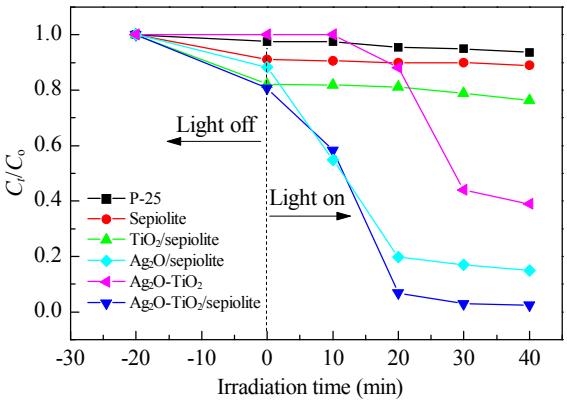

Fig. 11. Visible-light photocatalytic degradation of ARG solution by different samples.

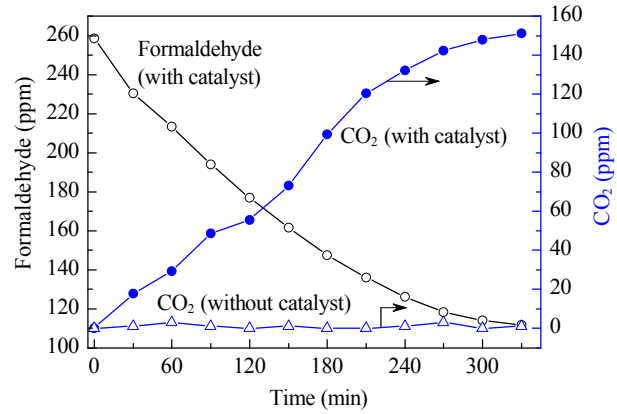

Fig. 12. Visible-light photocatalytic degradation of formaldehyde with and without Ag_2O-TiO_2/sepiolite catalyst.

based on multiphase heterostructures, which exist in this coordination to improve the photocatalytic activities of the composites. Formaldehyde, which is a typical volatile organic compound, was selected to further evaluate the photocatalytic properties of the Ag_2O-TiO_2/sepiolite composites.

Fig. 12 shows the photocatalytic degradation of gaseous formaldehyde under visible-light irradiation. The concentration of formaldehyde in air was reduced and the decomposition product of CO_2 gas was gradually increased with an increase in the irradiation time. Meanwhile, Fig. 12 also shows the results of a blank contrast experiment for gas formaldehyde exposed to visible light without catalyst, implying that the catalyst was critical for the degradation of gaseous formaldehyde to occur. These results suggest that the Ag_2O-TiO_2/sepiolite composite also exhibits relatively high photocatalytic activity for the degradation of gaseous formaldehyde under visible-light illumination.

3.3. Photocatalytic mechanism

Photoinduced active species ($^{\bullet}OH$, h^+, and $O_2^{\bullet-}$) are very important for the mineralization of organic contaminants. Therefore, the terephthalic acid photoluminescence (TAPL) technique was conducted to detect the formation of $^{\bullet}OH$. Scavengers were also employed to determine the oxidative species during the photocatalytic degradation process. As shown in Fig. 13(a), the intensity of the peaks increased slightly with an increase in the illumination time, indicating that $^{\bullet}OH$ was not the dominant species for the degradation of ARG solution. From Fig. 13(b), $^{\bullet}OH$ radicals trapping experiments (IPA) further determine that the $^{\bullet}OH$ was not the main active species in the photocatalytic process. KI was used as the scavenger of h^+ and $^{\bullet}OH$, sodium oxalate ($Na_2C_2O_4$) as the scavenger of h^+, and benzoquinone (BQ) as the scavenger of $O_2^{\bullet-}$ [60]. It can be seen that the KI and $Na_2C_2O_4$ had significant effects on the photocatalytic activity of the Ag_2O-TiO_2/sepiolite composite, which indicates that the h^+ is one of the main active species in the photocatalytic system. In the presence of BQ, the degradation efficiency of Ag_2O-TiO_2/sepiolite largely decreased, which suggests that $O_2^{\bullet-}$ is also one of the major active species in the photocatalytic system. $O_2^{\bullet-}$ could be generated by the adsorbed oxygen molecule on the surface of the catalyst capturing active electrons [26]. Thus, oxidative $h^+/O_2^{\bullet-}$ radicals could play an important role in the photocatalytic solution under visible-light irradiation and in the photocatalytic ARG degradation ability of the composite capturing the reactive species h^+, $^{\bullet}OH$, and $^{\bullet}O_2^-$.

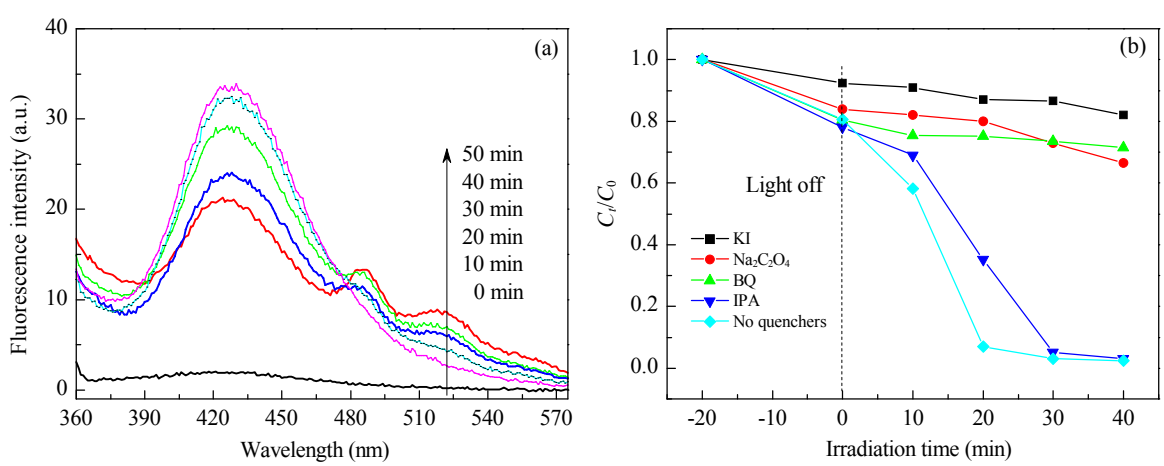

Fig. 13. (a) $^{\bullet}OH$ trapping PL spectra of terephthalic acid (TA) solution in the presence of the Ag_2O-TiO_2/sepiolite composite; (b) Photocatalytic degradation of ARG over the Ag_2O-TiO_2/sepiolite with and without the quenchers.

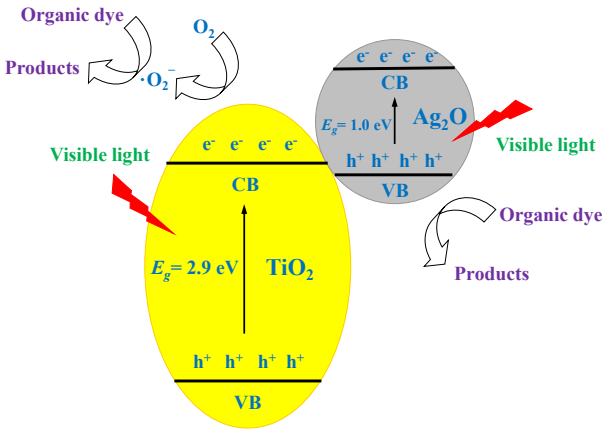

Fig. 14. Proposed photocatalytic mechanism of Ag_2O-TiO_2/sepiolite catalysts for the degradation of ARG solution under irradiation of visible light.

The enhanced photocatalytic mechanism of Ag_2O-TiO_2/sepiolite heterostructure is presented in Fig. 14. The high photocatalytic activity of the Ag_2O-TiO_2/sepiolite composite can be attributed to Ag_2O-TiO_2 heterostructure being in the composite and the porous structure of sepiolite. Under visible-light irradiation, Ag_2O nanoparticles can be excited to h^+ and e^- because of their narrow band gap. Meanwhile, Ag_2O has excessive negative charges that can easily adsorb onto positively charged TiO_2 nanoparticles [48,61,62]. In this case, the photogenerated electrons on the CB of Ag_2O can transfer into the CB of TiO_2 and the photogenerated holes gather in the VB of Ag_2O. Finally, the migration of photogenerated carriers is promoted because of the difference in band positions between those in the Ag_2O-TiO_2 heterojunction. Thereafter, the photogenerated electrons on the surface of Ag_2O can transfer into the CB of the TiO_2 that has reacted with molecular oxygen to produce $O_2^{\bullet-}$, and the holes generated in Ag_2O directly oxidize the adsorbed dyes or participate in the reaction to generate other radical species that oxidize the organic compounds. Thus, the series of oxidation-reduction reactions caused by the heterostructure of Ag_2O-TiO_2 can restrain the fast recombination of photoinduced electron-hole pairs effectively. Meanwhile, the porous structure of the sepiolite clay provides numerous nucleation sites for the formation of Ag_2O-TiO_2 heterostructure. This synergistic effect leads to the enhancement in photocatalytic activity [63].

4. Conclusions

Novel Ag_2O-TiO_2/sepiolite composites with heterostructure were synthesized by a simple two-step method. The as-prepared Ag_2O-TiO_2/sepiolite composites exhibited enhanced visible-light photocatalytic activity for the degradation of ARG. This enhancement may be ascribed to the porous structure of sepiolite and the high quantum efficiency of Ag_2O-TiO_2 heterostructure. Under visible-light irradiation, Ag_2O nanoparticles as a visible-light active component enhanced the Ag_2O-TiO_2 heterostructure photocatalytic activity via synergetic effects on the electron-hole separation and efficient electron transmission at the Ag_2O-TiO_2 interface. Sepiolite clay as the substrate for Ag_2O-TiO_2 heterostructure could provide more active sites and enhance the adsorption properties. In addition, the h^+ and $O_2^{\bullet-}$ radicals could be the main active species during the photo-oxidation process. This result may provide a new strategy for the design and development of high-performance visible-light photocatalysts.

References

[1] Wang H, Yuan X Z, Wu Y, Zeng G M, Chen X H, Leng L J, Wu Z B, Jiang L B, Li H. *J Hazard Mater*, 2015, 286: 187
[2] Liu J, Zhang G K. *Appl Surf Sci*, 2014, 319: 291
[3] Mehrjouei M, Müller S, Möller D. *Chem Eng J*, 2015, 263: 209
[4] Yang Y Q, Zhang G K, Yu S J, Shen X. *Chem Eng J*, 2010, 162: 171
[5] Liu Y P, Fang L, Lu H D, Liu L J, Wang H, Hu C Z. *Catal Commun*, 2012, 17: 200
[6] Liu J, Zhang G K. *Phys Chem Chem Phys*, 2014, 16: 8178
[7] He F, Ma F, Li T, Li G X. *Chin J Catal*, 2013, 34: 2263
[8] Yang Y Q, Zhang G K, Xu W. *J Colloid Interface Sci*, 2012, 376: 217
[9] Yu J G, Xiong J F, Cheng B, Liu S W. *Appl Catal B*, 2005, 60: 211
[10] Cao X Y, Oda Y, Shiraishi F. *Chem Eng J*, 2010, 156: 98
[11] Pelaez M, de la Cruz A A, Stathatos E, Falaras P, Dionysiou D D. *Catal Today*, 2009, 144: 19
[12] Araña J, Peña Alonso A, Doña Rodríguez J M, Herrera Melián J A, González Díaz O, Pérez Peña J. *Appl Catal B*, 2008, 78: 355
[13] He X, Tang A D, Yang H M, Ouyang J. *Appl Clay Sci*, 2011, 53: 80
[14] Zhao W, Chen C C, Li X Z, Zhao J C, Hidaka H, Serpone N. *J Phys Chem B*, 2002, 106: 5022
[15] He R A, Cao S W, Zhou P, Yu J G. *Chin J Catal*, 2014, 35: 989
[16] Xu J, Wang G X, Fan J J, Liu B S, Cao S W, Yu J G. *J Power Sources*, 2015, 274: 77
[17] Tang A D, Jia Y R, Zhang S Y, Yu Q M, Zhang X C. *Catal Commun*, 2014, 50: 1
[18] Lee S S, Bai H W, Liu Z Y, Sun D D. *Water Res*, 2013, 47: 4059
[19] Chen L, Hua H, Yang Q, Hu C G. *Appl Surf Sci*, 2015, 327: 62
[20] Yu C L, Zhou W Q, Yu J C, Liu H, Wei L F. *Chin J Catal*, 2014, 35: 1609
[21] Hsu M H, Chang C J. *J Hazard Mater*, 2014, 278: 444
[22] Goei R, Lim T T. *Water Res*, 2014, 59: 207
[23] Zhou W J, Liu H, Wang J Y, Liu D, Du G J, Cui J J. *ACS Appl Mater Interfaces*, 2010, 2: 2385
[24] Bouzid H, Faisal M, Harraz F A, Al-Sayari S A, Ismail A A. *Catal Today*, 2015, 252: 20
[25] Guo Y D, Zhang G K, Liu J, Zhang Y L. *RSC Adv*, 2013, 3: 2963
[26] Gan H H, Zhang G K, Guo Y D. *J Colloid Interface Sci*, 2012, 386: 373
[27] You Y, Wan L, Zhang S Y, Xu D F. *Mater Res Bull*, 2010, 45: 1850
[28] Jiang B, Jiang L L, Shi X W, Wang W C, Li G S, Zhu F X, Zhang D Q. *J Sol-Gel Sci Technol*, 2015, 73: 314
[29] Hua H, Xi Y, Zhao Z H, Xie X, Hu C G, Liu H. *Mater Lett*, 2013, 91: 81
[30] Ren H T, Jia S Y, Zou J J, Wu S H, Han X. *Appl Catal B*, 2015, 176–177: 53
[31] Kerkez O, Boz I. *Chem Eng Commun*, 2015, 202: 534
[32] Valentín J L, López-Manchado M A, Rodríguez A, Posadas P, Ibarra L. *Appl Clay Sci*, 2007, 36: 245
[33] Jung K Y, Park S B. *J Photochem Photobiol A*, 1999, 127: 117
[34] Zhang G K, Xiong Q, Xu W, Guo S. *Appl Clay Sci*, 2014, 102: 231
[35] Chen F T, Liu Z, Liu Y, Fang P F, Dai Y Q. *Chem Eng J*, 2013, 221: 283
[36] Akgun B A, Durucan C, Mellott N P. *J Sol-Gel Sci Technol*, 2011, 58: 277

Graphical Abstract

Chin. J. Catal., 2015, 36: 2219–2228 doi: 10.1016/S1872-2067(15)61015-4

Facile synthesis of Ag_2O-TiO_2/sepiolite composites with enhanced visible-light photocatalytic properties

Yu Du, Dandan Tang, Gaoke Zhang*, Xiaoyong Wu
Wuhan University of Technology

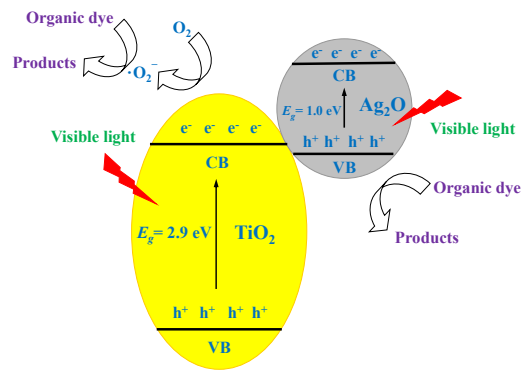

Under visible-light irradiation, the photo-generated electrons on the surface of Ag_2O would transfer into the conduction band (CB) of TiO_2 and then reacted with O_2 molecules to generate $\cdot O_2^-$. The organic dye was degraded by the photo-generated holes and $\cdot O_2^-$ active species.

[37] Zhang Y L, Wang D J, Zhang G K. *Chem Eng J*, 2011, 173: 1
[38] Stathatos E, Lianos P, Falaras P, Siokou A. *Langmuir*, 2000, 16: 2398
[39] Hussain S T, Rashid, Anjum D, Siddiqa A, Badshah A. *Mater Res Bull*, 2013, 48: 705
[40] Yu H G, Liu R, Wang X F, Wang P, Yu J G. *Appl Catal B*, 2012, 111–112: 326
[41] Arabatzis I M, Stergiopoulos T, Bernard M C, Labou D, Neophytides S G, Falaras P. *Appl Catal B*, 2003, 42: 187
[42] Yu J C, Yu J G, Zhang L Z, Ho W K. *J Photochem Photobiol A*, 2002, 148: 263
[43] Mei F, Liu C, Zhang L, Ren F, Zhou L, Zhao W K, Fang Y L. *J Cryst Growth*, 2006, 292: 87
[44] Lalitha K, Reddy J K, Sharma M V P, Kumari V D, Subrahmanyam M. *J Hydrogen Energy*, 2010, 35: 3991
[45] Hou X G, Huang M D, Wu X L, Liu A D. *Chem Eng J*, 2009, 146: 42
[46] Prieto P, Nistor V, Nouneh K, Oyama M, Abd-Lefdil M, Díaz R. *Appl Surf Sci*, 2012, 258: 8807
[47] Nicole J, Tsiplakides D, Pliangos C, Verykios X E, Comninellis C, Vayenas C G. *J Catal*, 2001, 204: 23
[48] Gan H H, Zhang G K, Huang H X. *J Hazard Mater*, 2013, 250–251: 131
[49] Toranzo R, Vicente M A, Bañares-Muñoz M A, Candia L M, Gil A. *Microporous Mesoporous Mater*, 1998, 24: 173
[50] Li F F, Jiang Y S, Xia M S, Sun M M, Xue B, Ren X H. *J Hazard Mater*, 2009, 165: 1219
[51] Belessi V, Lambropoulou D, Konstantinou I, Katsoulidis A, Pomonis P, Petridis D, Albanis T. *Appl Catal B*, 2007, 73: 292
[52] Luckham P F, Rossi S. *Adv Colloid Interface Sci*, 1999, 82: 43
[53] Mora M, Isabel López M, Ángeles Carmona M, Jiménez-Sanchidrián C, Rafael Ruiz J. *Polyhedron*, 2010, 29: 3046
[54] Uğurlu M, Karaoğlu M H. *Chem Eng J*, 2011, 166: 859
[55] Demirbas A, Sari A, Isildak O. *J Hazard Mater*, 2006, 135: 226
[56] Uğurlu M. *Microporous Mesoporous Mater*, 2009, 119: 276
[57] Madejova J. *Vib Spectrosc*, 2003, 31: 1
[58] Amarjargal A, Tijing L D, Kim C S. *Ceram Int*, 2012, 38: 6365
[59] Ollis D F. *Environ Sci Technol*, 1985, 19: 480
[60] Wan Z, Zhang G K. *J Mater Chem A*, 2015, 3: 16737
[61] Li Q, Xie R C, Mintz E A, Shang J K. *J Am Ceram Soc*, 2007, 90: 3863
[62] Damm C, Herrmann R, Israel G, Müller F W. *Dyes Pigments*, 2007, 74: 335
[63] Priya R, Baiju K V, Shukla S, Biju S, Reddy M L P, Patil K R, Warrier K G K. *Catal Lett*, 2009, 128: 137

Page numbers refer to the contents in the print version, which include both the English version and extended Chinese abstract of the paper. The online version only has the English version. The pages with the extended Chinese abstract are only available in the print version.